Quaternary Geochronology 83 (2024) 101567

Contents lists available at ScienceDirect

Quaternary Geochronology

journal homepage: www.elsevier.com/locate/quageo

Extended-range luminescence and ESR dating of Iberian fluvial terraces (Duero and Guadiana basins) associated with the Lower Palaeolithic sites of La Maya I, II, III, Burganes and Albalá (west-central Spain)

Martina Demuro [a,*], Lee J. Arnold [a], Mathieu Duval [b,c,d], Alicia Churruca Clemente [b], Manuel Santonja [e], Alfredo Pérez-González [e]

[a] School of Physics, Chemistry and Earth Sciences, University of Adelaide, Adelaide, Australia
[b] Centro Nacional de Investigación sobre la Evolución Humana (CENIEH), Burgos, Spain
[c] Australian Research Centre for Human Evolution (ARCHE), Griffith University, Nathan, Australia
[d] Palaeoscience Labs, Dept. Archaeology and History, La Trobe University, Melbourne, Australia
[e] Instituto de Evolución en África (IDEA), Madrid, Spain

ARTICLE INFO

Keywords:
Single-grain TT-OSL
Post IR-IRSL
ESR dating
Acheulean
Fluvial terraces
Iberian Peninsula

ABSTRACT

The major river basins of the Iberian Peninsula that drain towards the Atlantic coast contain extensive Lower Palaeolithic (Acheulean) records associated with well-preserved fluvial terrace sequences. These open-air archaeological records are often difficult to constrain chronologically due to a lack of suitable material for dating (e.g., faunal remains) or because their Middle Pleistocene antiquity precludes the use of otherwise routinely applicable geochronometric techniques such as conventional optically stimulated luminescence (OSL) dating. As a result, many important Iberian Acheulean sites lack precise and accurate chronologies, and their existing temporal frameworks are based solely on morphostratigraphic correlations with regional fluvial terrace systems. Here we present the first application of extended-range luminescence dating – namely multi-grain post-infrared infrared stimulated luminescence (pIR-IRSL) dating of K-feldspars and single-grain thermally transferred-OSL (TT-OSL) dating of quartz – to a series of terrace sequences in the Duero basin (central sector) and Guadiana basin, as well as associated Lower Palaeolithic sites of La Maya I, II and III along the Tormes River, Burganes (and related sites) along the Tera River, and Albalá along the Guadiana River. Additionally, we present results of a parallel electron spin resonance (ESR) quartz dating study of the Tormes River terrace (Duero basin), which has been undertaken independently on the same samples to enable stratigraphically paired dating comparisons. Our study indicates that sedimentary quartz from this sector of the Duero basin produces very weak TT-OSL signals, variable Al signal repeatability and below-average Ti signal fitting uncertainties, though it is still possible to determine consistent comparative ages using the measurements protocols employed here. For samples where both pIR-IRSL and TT-OSL signals were measured, the paired luminescence dating ages are in agreement at 1σ. Agreement between the quartz ESR and TT-OSL ages is also observed for one sample from the Tormes River. However, the ESR signals (both Al and Ti) of a second sample showed insufficient bleaching and age overestimation in comparison to the paired TT-OSL dataset. Comparison of our latest dating results with published chronological datasets point to some fluvial terraces of the Duero basin potentially having diachronous formation histories. Despite this, our combined chronological results show that the terrace systems are chronologically ordered and suggest that, regionally, the +8 to +34 m terraces likely post-date marine isotope stage (MIS) 10, whilst the +50 m terraces formed prior to, or during, MIS 10. The related Acheulean sites that contain lithic material in stratigraphic position are dated to MIS 9–7 (193–314 ka at 2σ age range), and temporally overlap with the early Middle Palaeolithic records in the Duero basin, also dated here to MIS 8–7 (or 159–259 ka at 2σ). Our results are consistent with previous observations regarding the chronological overlap of these two technologies in the region, and support the possibility of a non-linear pattern of replacement for the Acheulean in the Iberian Peninsula during the Lower to Middle Palaeolithic transition.

* Corresponding author.
E-mail address: martina.demuro@adelaide.edu.au (M. Demuro).

https://doi.org/10.1016/j.quageo.2024.101567
Received 15 November 2023; Received in revised form 24 April 2024; Accepted 10 June 2024
Available online 26 June 2024

1. Introduction

A significant proportion of the Lower Palaeolithic (Acheulean) records from the Iberian Peninsula are associated with fluvial terrace sequences of the major river basins that drain into the Atlantic; particularly the Duero, Tagus, Guadiana (Santonja and Villa, 2006), Miño (Méndez-Quintas et al., 2018, 2019), and, to a lesser extent, the Guadalquivir (García-Vadillo et al., 2023) drainage systems. Unfortunately, these open-air archaeological records are often difficult to constrain chronologically due to a lack of suitable material for dating (e.g., calcite formation, faunal remains, well-preserved organics) or because they lie beyond the upper dating limits of commonly employed (often commercially sourced) sedimentary geochronometric techniques, such as multi-grain quartz optically stimulated luminescence (OSL) dating or radiocarbon dating. As a result, many important Middle Pleistocene Acheulean sites of the Iberian meseta lack precise and accurate chronologies, and their existing temporal frameworks are based on either morphostratigraphic correlations with regional fluvial terrace systems (Santonja and Villa, 2006; Santonja and Pérez-González, 2010) or, where available, macro- and micromammal faunal assemblages found in association with archaeological materials (e.g., Panera et al., 2014; Laplana et al., 2015; Rubio-Jara et al., 2016); though the latter is typically not a viable option owing to the poor preservation of fossil remains at most Iberian fluvial terrace sites (e.g., the Guadiana basin sites; Santonja and Villa, 2006).

Over the past two decades, luminescence and/or electron spin resonance (ESR) dating of silicates (quartz and potassium feldspars) has been employed in a number of geochronology studies of fluvial terraces from major tributaries of the Duero basin (Moreno et al., 2012, 2016; Arnold et al., 2013; Terradillos-Bernal et al., 2023), Miño basin (Méndez-Quintas et al., 2018, 2019; Demuro et al., 2020a, 2020b) and Tagus basin (Cunha et al., 2008; Martins et al., 2009, 2010; Panera et al., 2011; López-Recio et al., 2015; Moreno et al., 2019), among others. These past studies were mainly focused on establishing chronological frameworks for fluvial incision rates and, in some cases, to determine the age of associated archaeological (Acheulean occupation) sites. Despite these efforts, most of the fluvial networks and associated archaeological sites within these Atlantic basins remain undated and there is very limited chronological information to assess Middle Pleistocene human occupation patterns across this important geographic region, especially from open-air sites.

In order to improve the chronological framework of fluvial deposits located in the middle reaches of the Duero and Guadiana basins (central-west Spain), as well as the Acheulean records of northern and central Iberia, we present the first application of extended-range luminescence dating of sediment samples (multi-grain post-infrared infrared stimulated luminescence (post IR-IRSL) dating of K-feldspars and single-grain thermally transferred-OSL (TT-OSL) dating of quartz) from fluvial terraces at selected localities within these catchments. Some of the samples studied are directly associated with important Lower Palaeolithic sites that were surveyed or excavated in the 1970-80's: namely, Burganes I to III and Olmillos I and II, both located within the Tera River terrace system, La Maya I to III, located within the Tormes River terrace system (Duero basin; Santonja and Pérez-González, 1984), and the site of Albalá, located on a terrace of the Guadiana River (Guadiana basin; Santonja and Villa, 2006). Additionally, subsets of prepared quartz grains from the luminescence dating samples of the Tormes River terraces are dated using ESR to enable stratigraphically paired, comparative age assessments.

The aim of this paper is to: (i) assess the suitability of extended-range luminescence signals for dating the Middle Pleistocene deposits of the Duero and Guadiana basins via the application of a series of quality assurance criteria (e.g., signal intensity assessments, dose recovery tests) and semi-independent ESR dating comparisons for selected samples; (ii) establish new multi-method chronologies and evaluate the accuracy of existing chronostratigraphic frameworks for the terrace sequences and associated archaeological sites, and (iii) assess the wider implications of the dating results for understanding Acheulean occupation patterns in the Iberian Peninsula more broadly.

2. Study sites and samples

Accessible locations with well-preserved stratigraphic exposures were targeted within the Tera, Tormes and Guadiana River basins (Fig. 1a) for luminescence and ESR sample collection. Further descriptions of geographic locations, fluvial terrace elevations and sedimentary sequence associated with each sampling site are outlined in the Supplementary Information. In total, three dating samples were collected from the +16–20 m and +30–34 m terraces of the Tera River, six samples were collected from the +8m, +14 m, +34 m and +50 m terraces of the Tormes River and two samples were collected from the +8 m terrace of the Guadiana River.

2.1. Tera River terraces (Duero basin)

The Tera River is located on the northern flank of the Duero basin, where it joins the Esla River and eventually drains into the midsection of the Duero, approximately 25 km to the west of the city of Zamora. Archaeological surveys were undertaken during the 1970-80's near the town of Burganes de Valverde (Zamora province), just prior to the confluence with the Esla River (Fig. 1b). The terrace system identified in this section of the Tera River is composed, in its lower part, of four terraces at +3–5 m, +10–12 m, +16–20 m and +30–35 m elevations above the river level. Surveying of the +16–20 m fluvial terrace revealed a series of archaeological sites located on the west margin of the river (Fig. 1; Santonja and Pérez-González, 1984). Four of these sites contained Acheulean assemblages in stratigraphic position, namely Burganes I and II and Olmillos I and II (see Fig. 1b), which were subsequently studied in detail. A fifth site, Burganes III, was also identified as containing exposed lithics within surficial deposits. Unlike the aforementioned four sites, the age of the Burganes III assemblage is considered to be younger than the formation of the +16–20 m fluvial terrace.

To chronologically constrain the Tera River terrace formations and associated Acheulean records, three luminescence dating samples were collected from exposures of fluvial deposits in the vicinity of the town of Burganes de Valverde and within the previously surveyed archaeological areas: one sample (BGN16-1; Fig. S1a) was collected from the +30–35 m terrace and two samples (BGN16-2 and BGN16-3; Figs. S1b–c) were collected from an exposure corresponding to the +16–20 m terrace (Fig. 1b).

2.2. Tormes River terraces (Duero basin)

The Tormes River is located on the southern flank of the Duero basin and joins the main Duero River at the border between Spain and Portugal. The present study focuses primarily on terrace formations and archaeological sites located to the south of the town of Santa Teresa de Tormes (Fig. 1c). In this section of the Tormes River, the better preserved terraces are at middle and lower elevations, mapped at +4–6 m, +8 m, +14 m, +30–32 m and +50–54 m above the river level (Fig. 1c; Santonja and Pérez-González, 1984). The middle-to-upper and upper terraces are poorly preserved due to erosion, though three to four extra terraces have been identified above the +50 m level, with the highest point at +100–110 m (Santonja and Pérez-González, 1984). Archaeological surveying undertaken in the 1970's identified the site of La Maya I within a quarry exposure, which contained archaeological material in stratigraphic position. La Maya I was subdivided into two excavation areas: a 12 m^2 excavation called 'Zona 1', which sits within the +14 m terrace, and a second 6 m^2 excavation area called 'Zona 2', which is located on the +8 m terrace. A further two sites, La Maya II and La Maya III, were also identified, though in both cases the archaeological material was found on top of the surface deposits capping the +30–32 m and +50–54 m terraces, respectively (see Fig. 1c; Santonja and Pérez-González, 1984). The lithic material found in all instances was classed as Acheulean, though the assemblage from the +8 m terrace excavation at La Maya I 'Zona 2' was deemed to exhibit certain characteristic elements of a late Acheulean or early Middle Palaeolithic (EMP) toolkit (Santonja and Villa, 2006).

In total, six luminescence and ESR dating samples were collected from the fluvial terrace system of the Tormes River (see Fig. S2). Due to a lack of stratigraphic exposures for the +50–54 m and +30–32 m terraces near Santa Teresa de Tormes, two correlative localities were identified 24 km downstream of the Tormes River near the town of Villargonzalo de Tormes (Fig. 1d). Further downstream from here, the terrace system is better preserved and the number of fluvial terraces identified increases significantly, including several higher terraces at +62–64 m, +78–80 m, +108 m and +120 m above river level (Fig. 1d; Santonja and Pérez-González, 1984). *In situ* and surficial archaeological material have also been studied in this sector of the Tormes (locations shown in Fig. 1d). Within this system, we collected three luminescence and ESR samples, LM18-1 and LM18-2 from the +50 m terrace, and LM16-1 from

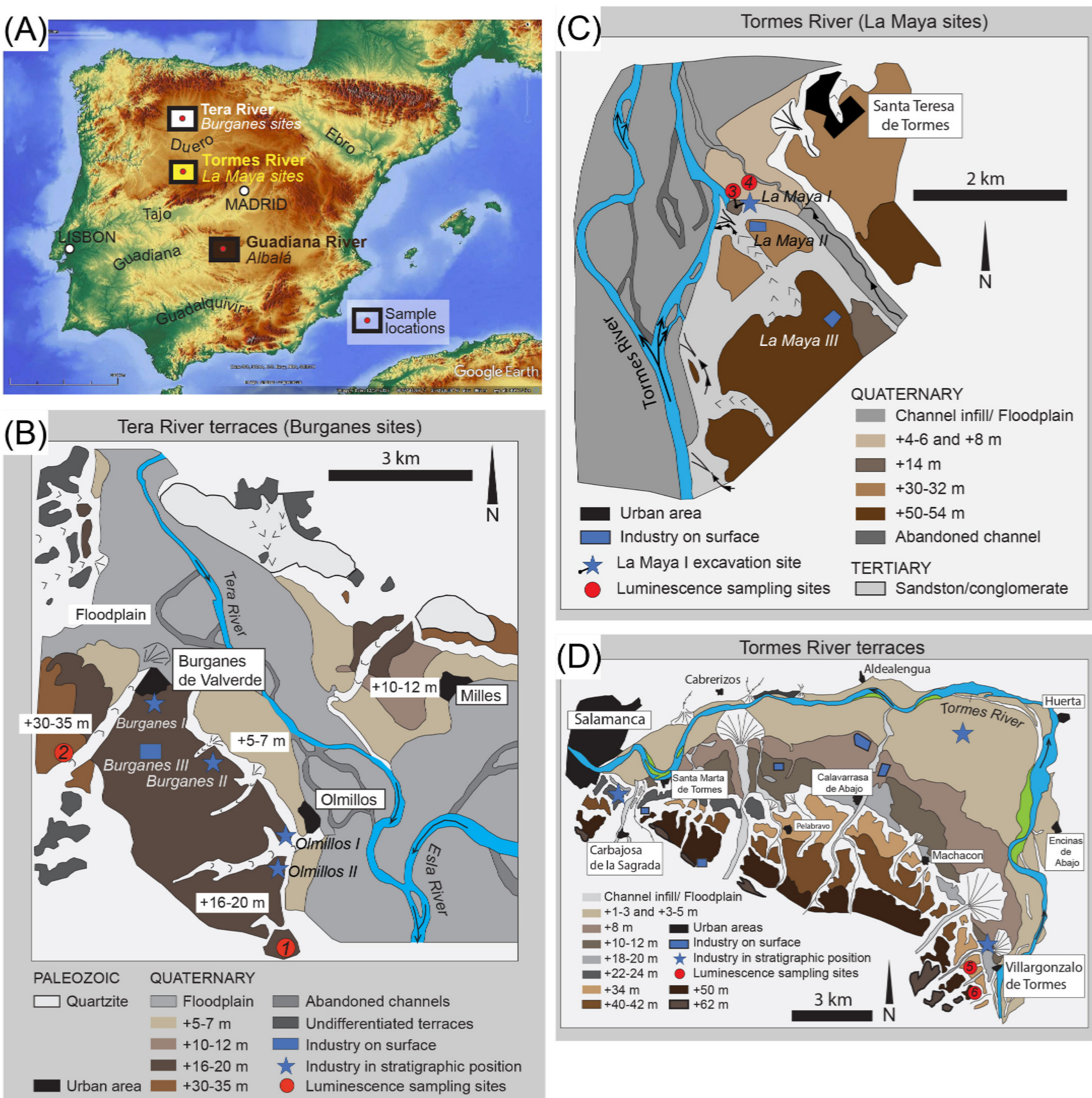

Fig. 1. Maps showing (A) the general location of study sites along the Tera, Tormes and Guadiana Rivers. Luminescence dating sampling locations within the Duero basin for the: (B) Tera River terraces at (1) +16–20 m and (2) +30–35 m elevation; (C) Tormes River terraces at (3) +14 m and (4) +8 m elevation; and (D) Tormes River terraces at (5) +34 m and (6) +50 m elevation. Also shown are the locations of associated archaeological sites La Maya I, II and III, Burganes I, II and III, and Olmillos I and II. Panels B–D have been modified from Santonja and Pérez-González (1984).

the +34 m the terrace (Figs. S2b and d). These three samples provide chronological control for the correlative terraces near the town of Santa Teresa de Tormes and maximum age constraint for the surficial archaeological material of La Maya II and III. Two luminescence dating samples were collected from the excavation exposures at La Maya I 'Zona 1' corresponding with the +14 m terrace: sample LM16-2 was collected from Level 'a' and sample LM16-3 from overlying Level 'b' (Fig. S2c). Finally, due to a lack of available exposures in La Maya I 'Zona 2', one luminescence dating sample, LM16-4, was collected from a nearby exposure of the +8 m terrace, which was located approximately 100 m away from the La Maya I 'Zona 2' site (Fig. S2a).

2.3. Guadiana River terrace (Guadiana basin)

The Guadiana River basin is an extensive fluvial network that runs parallel to the Tagus River and drains a large portion of the meridional meseta. However, the Guadiana terrace system exhibits less vertical development (Santonja and Pérez-González, 2010) and fewer Lower Palaeolithic archaeological sites than in neighbouring basins to the north (Santonja and Villa, 2006). Despite this, several important Acheulean sites have been discovered and studied since the 1970's within the Campo de Calatrava region, an area located in the mid-section of the Guadiana River near the city of Ciudad Real (Santonja and Villa, 2006; Santonja et al., 2022). Previous studies have identified at least ten terrace levels in the Guadiana River basin, from +2 to 3 m to +60–65 m elevation (Portero et al., 1986; Santonja et al., 2022). The studied archaeological sites with Acheulean assemblages include El Martinete (on the +11–13 m terrace) and Albalá (on the +8 m terrace). Other important Acheulean sites in the area, including El Sotillo and Porzuna (Santonja and Villa, 2006; Arroyo and de la Torre, 2013; Santonja et al., 2022), are located a few kms to the north of the Guadiana River and are not directly associated with its terrace system. So far, the only chronology available for these Early Palaeolithic occupations in the Campo de Calatrava region comes from the site of El Sotillo, which has been dated to 258–303 ka using multi-grain K-feldspar pIR-IRSL and single-grain quartz TT-OSL (Santonja et al., 2022).

Two luminescence dating samples, ALB17-1 and ALB17-2, were collected from fluvial deposits of the +8 m Guadiana River terrace at a laterally continuous (>20 m) exposure (2–3 m thick) located on a road cutting, between the towns of Piedrabuena and Pozuelos. The fluvial deposits here are >7 m thick. Sample ALB17-1 was collected from a lower layer composed of cobbles and gravels, while sample ALB17-2 was collected from an overlaying layer composed predominantly of sands (see Supplementary Information for details; Figs. S3a–d).

3. Methods

3.1. Luminescence D_e determination

All samples were dated using replicate K-feldspar pIR-IRSL and quartz TT-OSL procedures, with the exception of Guadiana River samples ALB17-1 and ALB17-2, which were only dated using pIR-IRSL procedures owing to the significantly longer measurement requirements of TT-OSL dating, and Tormes River sample LM18-1, which was principally prepared for ESR dating and not measured for pIR-IRSL or TT-OSL dating owing to machine time limitations. Full details of the luminescence dating procedures and instrumentation employed in this study (including quality assurance criteria used to eliminate unreliable grains and aliquots) are provided in the Supplementary Information. The 90–125 μm fractions of K-feldspar and quartz concentrates were prepared using standard preparation procedures (e.g., Demuro et al., 2014) including HF acid etching to remove the alpha-irradiated external layers (10% HF digestion for 10 min to etch the K-feldspar fractions; 48% HF digestion for 40 min to etch the quartz fractions; Aitken, 1998; Duval et al., 2017). Multi-grain pIR-IRSL and single-grain TT-OSL measurements were made using the single-aliquot regenerative-dose (SAR) protocols (Murray and Wintle (2000) detailed in Arnold et al., 2014, 2019) and Demuro et al. (2015, 2019a, 2019b, 2022), and shown in Tables S1a–b. The pIR-IRSL procedure makes use of raised temperature stimulation at 225 °C after a preheat of 250 °C for 60 s, and is herein denoted pIR-$IRSL_{225}$. The suitability of these SAR procedures for D_e determination is supported by reliable dose-recovery test results for the quartz fraction of sample LM16-3 (TT-OSL signal) and K-feldspar fractions of samples LM16-2, BGN16-1 and ALB17-1 (pIR-$IRSL_{225}$ signal), as outlined in the Supplementary Information and Tables S2–S3.

Grains or aliquots that passed the SAR rejection criteria described in the Supplementary Information were used for final D_e estimation and age calculation (Table S6). Representative burial dose estimates have been calculated using the central age model (CAM), and the 3-parameter and 4-parameter minimum age models (MAM-3 and MAM-4) of Galbraith et al. (1999). The choice of model to use for the final age calculations has been made on statistical grounds using the overdispersion parameter (calculated using the CAM) and the maximum log likelihood, L_{max}, criterion of Arnold et al. (2009) (to ascertain the statistical appropriateness of the MAM-3 versus MAM-4), and by taking into consideration the depositional context of these samples (i.e., fluvial settings with direct or indirect sub-aerial exposure between transportation events), as well as the different bleaching characteristics of the various luminescence signals under consideration (Arnold et al., 2013, 2019, 2022; Demuro et al., 2015; Duval et al., 2017).

3.2. ESR D_e determination

ESR dating of quartz grains was undertaken on four samples collected from the Tormes River fluvial deposits. The unused coarse quartz grain fractions of samples LM16-1 (180–250 μm), LM16-4 (180–250 μm), LM18-1 (125–212 μm) and LM18-2 (125–250 μm) prepared as part of the luminescence dating study were selected for ESR dating. ESR dose evaluation was performed at the National Research Centre for Human Evolution (CENIEH), Spain, using published analytical procedure and experimental conditions (e.g., Duval et al., 2020a). Quartz grains were dated using the multiple aliquot additive dose (MAAD) method and following the multiple centre (MC) approach defined by Toyoda et al. (2000). ESR measurements were carried out at 90–92 K, with an EMXmicro 6/1Bruker X-band ESR spectrometer coupled to a standard rectangular ER 4102ST cavity (setup #1 in Guilarte and Duval, 2021).

For all samples, the ESR signals of the Aluminium (Al) and Titanium (Ti) centres were acquired in a single spectrum (e.g., Fig. S6). Detailed acquisition parameters and experimental conditions are outlined in the Supplementary Information. The ESR intensity of the Al signal was extracted from peak-to-peak amplitude measurements between the top of the first peak (g = 2.0185) and the bottom of the last peak at g values between ~2.018 and ~1.993 (Toyoda and Falguères, 2003). The ESR intensity of the Ti centres was measured from the peak-to-baseline amplitude of the peak at g = 1.913 (i.e., option D *sensu* Duval and Guilarte, 2015). For completeness, the ESR intensities were also measured following options A, C and E *sensu* Duval and Guilarte (2015), although the fitting results are not discussed here (see Supplementary Information and Table S12). The final Dose Response Curves (DRCs) were obtained by plotting the mean ESR intensities and associated standard deviations derived from the repeated measurements. The DRC fitting conditions are described in the Supplementary Information.

3.3. Environmental dose rates

Environmental dose rates for both the luminescence and ESR dating calculations were determined via a combination of *in situ* field gamma-ray spectrometry and low-level beta counting (Table S4). The 'energy windows' method described in Arnold et al. (2012a) and Duval and Arnold (2013) has been used to analyse the field gamma spectra and determine radionuclide concentrations of K, U and Th for the surrounding sediment matrices. External gamma dose rates have been calculated using the conversion factors of Guérin et al. (2011). External beta dose rates have been derived from laboratory measurements of homogenised sediment sub-samples collected immediately adjacent to the luminescence dating samples using a Risø GM-25-5 beta counter. Contributions from cosmic rays have been calculated using the approach described in Prescott and Hutton (1994). An internal ^{40}K content of 12.5 ± 0.5% (Huntley and Baril, 1997) and ^{87}Rb content of 400 ± 100 ppm (Huntley and Hancock, 2001) have been assumed for determining the internal dose rates of K-feldspar grains. An internal dose date of 0.03 Gy/ka was assumed for quartz grains following previous publications (see footnote 'e' in Table S4).

The present-day sediment water contents of these samples are not considered to be entirely representative of true moisture conditions prevailing throughout the burial period because the exposed sediment profiles had partially dried out prior to sampling and fieldwork was conducted during the drier summer months. To determine more suitable long-term sediment moisture contents for dose rate determination, we have used 60% of the present-day saturated water contents, consistent with the long-term average water contents adopted for similar types of deposits from the Iberian Peninsula (e.g., Arnold et al., 2013; Demuro et al., 2015; Méndez-Quintas et al., 2018; Rios-Garaizar et al., 2022; Santamaría et al., 2023; Terradillos-Bernal et al., 2023). This approach resulted in long-term moisture contents ranging from 9.8% to 20.3% (as percentage of dry weight) depending on the sample (Table S4). A 1σ relative uncertainty of ±20% (±40% at 2σ) was assigned to these long-term estimates to account for any past variations in hydrological conditions during burial. High-resolution gamma spectrometry was additionally performed on a subset of representative samples from each basin to assess the state of secular equilibrium in the ^{238}U and ^{232}Th day series (Table S5). The daughter-parent isotopic ratios for ^{238}U, ^{226}Ra, ^{210}Pb, ^{228}Ra and ^{228}Th are consistent with unity at either 1σ or 2σ for all samples, confirming that the ^{238}U and ^{232}Th chains exhibit present-day secular equilibrium.

4. Results

4.1. Luminescence dating

The measured single-grain TT-OSL signals were generally very weak; approximately 71–86% of grains did not produce detectable luminescence (i.e., T_n signal <3 × signal background; Table S6) and a further 10–18% of grains displayed dim T_n signals with large associated errors of >30% (Table S6). The three Tera River samples (BGN16-1, BGN16-2 and BGN16-3) displayed the weakest TT-OSL signals, followed by the Tormes River samples LM18-2, LM16-1 and LM16-4 (brightest 1% of grains produced 0.10–3 counts/Gy/0.26 s; Fig. 2a). Samples LM16-2 and LM16-3, both from the +14 m terrace of the Tormes River, had marginally stronger TT-OSL signals (brightest 1% of grains produced 1–9 counts/Gy/0.26 s; Fig. 2a). The proportion of measured grains per sample that passed the single-grain TT-OSL SAR rejection criteria was generally very low, between 0.7 and 1.6% in most cases, though for samples LM16-2 and LM16-3 the yield of useable grains was slightly higher at 2.5% and 5% of measured grains, respectively (Table S6). Despite this, all TT-OSL signals used for D_e estimation were fast-decaying and generally depleted by >90% within the first 0.26 s of stimulation. An example of a sensitivity-corrected dose-response and TT-OSL decay curve for a moderately bright grain that passed the SAR rejection criteria is shown in Fig. 2b. The single-grain TT-OSL dose-response curves are all well-represented by a single saturating exponential function and display continued signal growth at high doses (>10^3 Gy) (Fig. 2b).

All pIR-IRSL$_{225}$ signals are bright and fast decaying, with the signals decreasing by >90% in the first 20 s of stimulation. Fig. 2c shows an example of a multi-grain pIR-ISL$_{225}$ decay curve and corresponding dose-response curve for sample LM18-2. The dose response curves are

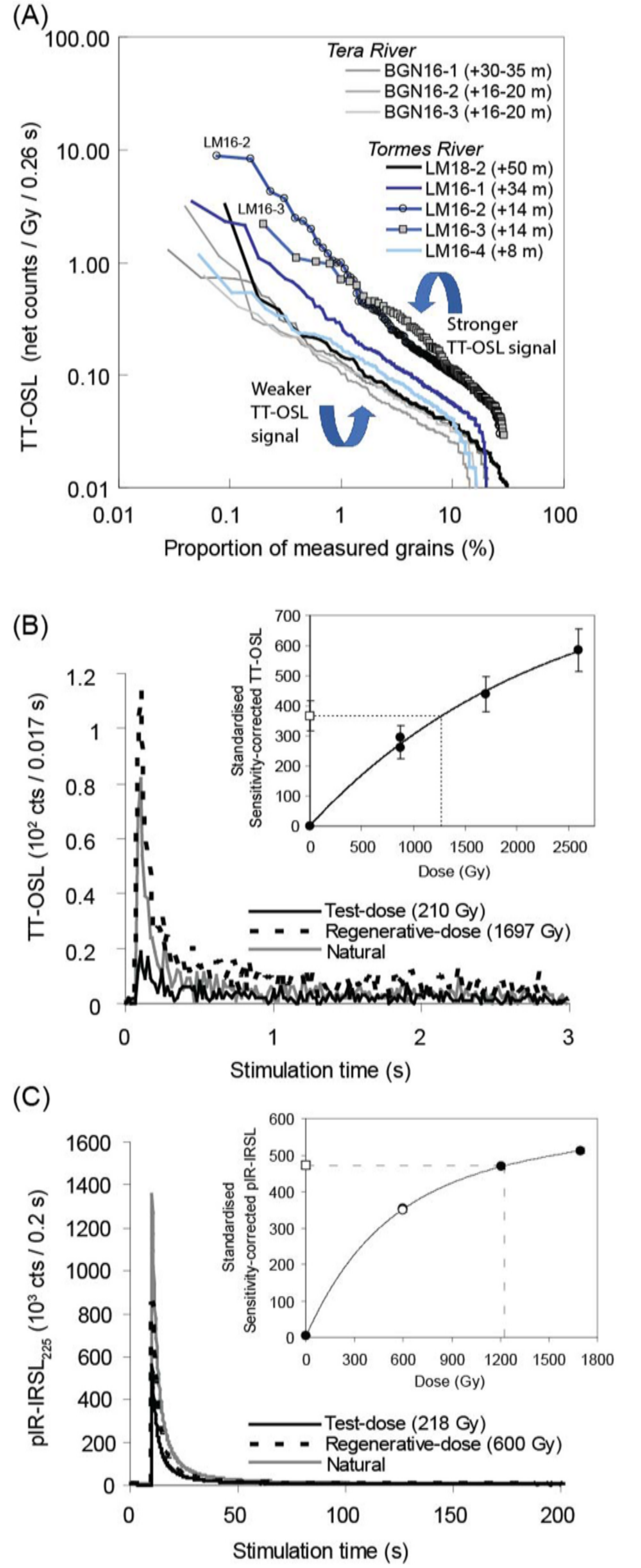

Fig. 2. (A) Single-grain TT-OSL signal brightness plot for samples collected from the Tera and Tormes River terraces. (B) Representative single-grain TT-OSL decay and sensitivity-corrected dose response curves measured, example shown is from a grain of sample LM16-1. (C) Representative multi-grain pIR-IRSL$_{225}$ decay and sensitivity-corrected dose response curves measured, example is from an aliquot of sample LM18-2.

optimally fitted using an exponential plus linear function. For the samples collected from the Tera and Guadiana River terraces, the D_e estimates were all calculated from the non-saturated portion of the dose response curves, though the D_e values for samples LM16-1, LM16-2, LM16-3 and LM18-2 from the Tormes River +34 m, +14 m, +14 m and +50 m terraces, respectively, were obtained from portions of the dose response curve that are closer to saturation (800–1200 Gy).

The degree of athermal loss of K-feldspar pIR-$IRSL_{225}$ signals over burial timescales was examined for all samples through anomalous fading assessments made on subsets of aliquots that had been used to derive D_e values (three aliquots per sample). The mean fading rates for individual samples generally range between 1.31 ± 0.15 and 1.90 ± 0.14 %/decade (with only one sample producing a higher value of 2.11 ± 0.19 %/decade) and the combined weighted average g-value ($n = 30$) is 1.64 ± 0.09 %/decade (Table S7). These empirical fading rates are consistent with those obtained for higher temperature pIR-IRSL signals (pIR-$IRSL_{290}$ signals) for a subset of the Tormes, Tera and Guadiana River terrace samples (mean value = 1.43 ± 0.09 %/decade; Table S7). More broadly, the measured fading rates for the pIR-$IRSL_{225}$ signals are also consistent with published g-values for higher temperature pIR-IRSL signals (see summary in Arnold et al., 2015), as well as published g-values for athermally stable quartz OSL signals (Buylaert et al., 2012), and they fall within the 1–2 %/decade range that is generally considered to be an artefact of laboratory procedures and potentially representing unreliable indicators of long-term fading rates (see discussions in Arnold et al., 2015). As such, we have not applied an empirical fading correction to the pIR-IRSL ages obtained in this study; though the fading corrected ages of a representative dataset (the Tormes terrace samples) are presented in the Supplementary Information and Table S8 for comparative purposes.

Sample LM18-2 (Tormes River +50 m terrace) could not be dated using single-grain TT-OSL because the measured grains consistently displayed weak or non-existent luminescence signals (i.e., ~94% of grains had unsuitably low T_n signals), or aberrant behaviour, and none of the measured grains passed the SAR quality assurance criteria. For the rest of the samples, a low, but sufficient, number of single-grain TT-OSL D_e values (22–35 grains per sample) passed the SAR quality assurance criteria and could be used to calculate an age. The single-grain TT-OSL D_e distributions of most samples are characterised by low to moderate scatter, with overdispersion values between 5% and 35%, which are consistent with those reported for well-bleached TT-OSL datasets (e.g., Arnold et al., 2019, 2022) (Table 1; Fig. S4). Only one sample, BGN16-2, exhibits an above-average overdispersion value of 51 ± 11%, albeit with a large uncertainty range (2σ uncertainty = ±22%) (Fig. S4f). For all samples, the D_e scatter is mostly randomly spread around the mean, with a few precise high and low D_e values for some datasets, and none of the D_e distributions display clear evidence of partial bleaching (i.e., there is a general absence of distinct leading-edges of low D_e values or elongated tails of higher D_e values; Arnold and Roberts, 2009; Bailey and Arnold, 2006) (see radial plots in Fig. S4 and D_e summary statistics in Table S9). Therefore, all final D_e values and age calculations have been determined using the CAM. This choice of age model is supported by the L_{max} scores obtained for the different age models, which indicate the CAM is statistically favoured over the MAM-3 and MAM-4 in all instances (Arnold et al., 2019), and the weighted skewness scores, which indicate that none of the samples are significantly positively skewed according to the criterion outlined by Arnold and Roberts (2009) (Table S9).

All pIR-$IRSL_{225}$ D_e datasets display low scatter, with overdispersion values ranging from 0% to 19%, and none of the samples display the typical asymmetric spread associated with partially bleached grain populations, as shown by the weighted skewness scores (see radial plots in Fig. S5 and Table S10). These characteristics suggest the pIR-$IRSL_{225}$ signals of all ten samples were likely well-bleached at deposition, consistent with the single-grain TT-OSL datasets, hence we have used the CAM D_e values for age determination. The suitability of the CAM over the MAM-3 and MAM-4 is further supported by the L_{max} scores obtained for these datasets (Arnold et al., 2019; Table S10).

4.2. ESR dating

The Al centre measurements for samples LM16-4 and LM18-2 reveal good repeatability of 5–10 % (Table S12), which are within standards

Table 1
Summary of single-grain TT-OSL and multi-grain pIR-$IRSL_{225}$ dating results for the Tera, Tormes and Guadiana River terrace samples.

Sample	Terrace elevation (m)	Single-grain TT-OSL[a]					Multi-grain pIR-$IRSL_{225}$[e]					Combined age (ka)[f]
		Accepted/ measured grains	OD (%)[b]	D_e (Gy)[c]	Total dose rate for Qz (Gy/ka)	Age (ka)[d]	Accepted/ measured aliquots	OD (%)[b]	D_e (Gy)[c]	Total dose rate for K-feldspars (Gy/ka)	Age (ka)[d]	
Tormes River												
LM16-4	+8	22/1900	29 ± 12	527 ± 55	2.52 ± 0.14	209 ± 25	6/6	4 ± 2	656 ± 14	2.98 ± 0.14	221 ± 12	219 ± 19
LM16-3	+14	25/500	23 ± 7	1019 ± 75	3.83 ± 0.20	266 ± 24	6/6	5 ± 2	1051 ± 25	4.29 ± 0.20	245 ± 14	250 ± 18
LM16-2	+14	32/1300	5 ± 21	971 ± 68	4.10 ± 0.24	237 ± 22	6/6	3 ± 2	1126 ± 23	4.56 ± 0.24	247 ± 15	244 ± 19
LM16-1	+34	35/2200	34 ± 7	972 ± 77	3.91 ± 0.20	249 ± 24	11/13	19 ± 5	1112 ± 72	4.37 ± 0.20	254 ± 21	252 ± 23
LM18-2	+50	0/1100	–	Not possible		–	15/15	0 ± 0	1168 ± 18	3.88 ± 0.18	323 ± 19	–
Tera River												
BGN16-3	+16-20	20/2400	37 ± 11	586 ± 63	2.64 ± 0.14	222 ± 27	15/15	6 ± 2	767 ± 14	3.10 ± 0.14	247 ± 13	242 ± 21
BGN16-2	+16-20	22/2500	51 ± 11	547 ± 69	2.62 ± 0.14	209 ± 29	12/12	8 ± 2	749 ± 18	3.07 ± 0.14	244 ± 14	237 ± 23
BGN16-1	+30-35	29/3600	31 ± 9	409 ± 36	1.37 ± 0.07	300 ± 30	6/6	10 ± 3	666 ± 27	1.82 ± 0.08	365 ± 22	342 ± 27
Guadiana River												
ALB17-2	+8	–	–	Not measured		–	9/9	14 ± 3	400 ± 19	1.77 ± 0.08	226 ± 15	–
ALB17-1	+8	–	–	Not measured		–	6/6	5 ± 2	487 ± 11	1.93 ± 0.08	252 ± 13	–

[a] TT-OSL measurements were made using the 'pseudo' single-grain approach (i.e., ~18 grains per hole; Arnold et al., 2012b).
[b] OD = overdispersion.
[c] D_e values have been calculated using the central age model (CAM; Galbraith et al., 1999).
[d] Mean ± total uncertainty (68% confidence interval), calculated as the quadratic sum of the random and systematic uncertainties. Total uncertainty includes a systematic component of ±2% associated with laboratory beta-source calibration.
[e] pIR-$IRSL_{225}$ measurements were made using 160-grain aliquots of 90–125 μm potassium feldspar grains.
[f] Weighted mean age has been calculated from the replicate TT-OSL and pIR-$IRSL_{225}$ ages for each sample. The associated 1σ uncertainty on the combined age has been calculated by multiplying the average relative uncertainties of the replicate age estimates by the combined weighted mean age estimate.

Table 2
Summary of the quartz ESR results for the four Tormes River samples. Dose rate components are given in Table S4. Final D_e values have been derived from either the Al signal (LM16-1) or by combining (as a weighted mean) the D_e values from the Al and Ti signals (see text for further explanations).

Sample	Terrace elevation (m)	D_e (Gy)	Total dose rate (Gy/ka)	Age (ka)
LM16-4	+8 m	970 ± 67 (Al–Ti)	2.41 ± 0.13	402 ± 36
LM16-1	+34 m	1082 ± 292 (Al)	3.76 ± 0.19	288 ± 79
LM18-1	+50 m	1945 ± 199 (Al–Ti)	4.67 ± 0.26	416 ± 50
LM18-2	+50 m	1441 ± 48 (Al–Ti)	3.33 ± 0.17	433 ± 28

for this signal (Duval et al., 2024). The exponential plus linear dose response curves for these two samples also show high goodness-of-fit values (adjusted $r^2 > 0.99$), and the resultant D_e estimates are in agreement at 1σ when using either the $1/I^2$ or $1/s^2$ weighing methods (Table S12). The repeated Al centre measurements for sample LM18-1 show slightly higher variations in D_e values (15–17%). It is worth noting that one of these measurements was erroneously performed with a microwave power of 0.6 mW instead of 5 mW, resulting in much smaller ESR intensities but with no significant impact on the resulting D_e estimate (Table 2). The exponential plus linear dose response curves obtained for LM18-1 using the two weighting options show regular goodness-of-fit values (adjusted r^2 ~0.98) and the resultant D_e estimates differ by about 20%, but are nevertheless in agreement at 1σ. Finally, the repeated Al centre measurements for sample LM16-1 show very low repeatability, with D_e estimates varying by ~54%. The D_e values obtained using the exponential plus linear dose response fittings vary by ~50% depending on the weighing method used (538 ± 209 Gy versus 1082 ± 292 Gy when using the $1/I^2$ and $1/s^2$ weighting, respectively; Table S12). There is evidence to suggest that the higher D_e value of 1082 ± 292 Gy obtained using the $1/s^2$ weighting is more reliable (see Fig. S7), namely (i) its goodness-of-fit value (adjusted r^2 = 0.997) is higher than that resulting from the $1/I^2$ weighted fitting (adjusted r^2 = 0.974), and (ii) the $1/I^2$ weighted fitting is more sensitive to biases caused by the significant scatter observed over the low dose points for this sample, as it gives higher weighting to the low dose region of the dose response curve (see Joannes-Boyau et al., 2018). Regardless, both Al centre D_e values for LM16-1 should be considered with extreme caution given the large variability observed over repeated measurements.

The Ti signal of samples LM16-4 and LM18-2 shows D_e repeatability within standards (i.e., between 0 and 15%, consistent with 90% of quartz samples in the synthesis study of Duval et al., 2024), and moderate to high goodness-of-fit values for the Ti-2 and single saturating exponential dose response curves (adjusted $r^2 < 0.98$ and >0.99, respectively). Both fittings return D_e estimates in agreement with each other at 1σ, though there is a ~250 Gy difference in the corresponding D_e values obtained for sample LM18-2 (Table S12). This D_e variability mostly reflects significant fitting uncertainty over the low dose region of the dose response curve (especially as the low dose points are scattered and the natural dose point is higher than the lowest irradiated dose point; see Fig. S8). In this case, the Ti-2 D_e value derived from all data points in the dose response curve, which shows a higher goodness-of-fit value, is regarded as more reliable than the D_e value obtained using the single saturating exponential fit, which is derived exclusively from the lower dose points (i.e., using a D_{max} of 9.7 kGy). For sample LM18-1, which shows slightly inferior repeatability of 17.2%, the Ti-2 and single saturating exponential dose response curve fitting methods yield D_e values in agreement at 1σ (2086 ± 365 Gy and 1850 ± 298 Gy; Table S12). These D_e estimates should nevertheless be treated with caution given their moderate goodness-of-fit values (adjusted r^2 values of 0.95–0.96; Table S12). However, the suitability of the Ti-2 fit improves (r^2 increases from 0.950 to 0.962) when excluding the scattered dose point at 9.7 kGy (Fig. S8), and the resultant D_e estimate comes into closer alignment with that obtained using the single saturating exponential function (i.e., 1850 ± 249 Gy; Table S12). Finally, sample LM16-1 shows very high Ti signal variability over repeated measurements (39%) but the D_e estimates obtained using the two fitting methods are in close agreement (1516.7 ± 173.9 Gy versus 1407.0 ± 247.6 Gy), with the Ti ($1/s^2$) fitting resulting in higher goodness-of-fit (Table S12). In general, the overall quality of the Ti signal dataset for these samples should be regarded as below usual standards (see compilation in Duval et al., 2024), with either low D_e precision over repeated measurements, regular goodness-of-fit, or non-negligible fitting uncertainties. The comparative results obtained in the present work for the Al and Ti signals also illustrate the limitations of the MAAD method for dose determination when ESR datasets do not meet routine quality standards.

Based on these observations, the Al centre ESR D_e values used for age evaluations are those obtained using an exponential plus linear dose response curve function fitting with $1/s^2$ weighting for sample LM16-1 and $1/I^2$ weighing for samples LM16-4, LM18-1 and LM18-2 (Table S12). The Ti centre ESR D_e estimate used for age evaluations are those derived from the Ti-2 ($1/s^2$) dose response curve fittings, which provide equally or more reliable fitting results than the alternative approaches for all samples (Table S12). Fig. 3 shows a comparison of the final D_e value obtained using the Al and Ti signals. Following the principles of the MC approach, the Al centre is expected to provide maximum burial dose estimates given its slower optical bleaching rate (Toyoda et al., 2000; Duval et al., 2017). In comparison, the Ti signal should yield a closer estimate of the true burial dose given its more rapid and complete bleaching characteristics. Samples LM16-4, LM18-1 and LM18-2 show the typical D_e pattern expected from the known relative bleaching rates of each signal (i.e., D_e (Ti) < D_e (Al)). For these three samples, the relative differences in the comparative Ti and Al D_e values are limited (varying by only −6 % to −16 %), and the paired D_e estimates are all within error, suggesting that the Al signal has been fully reset prior deposition, as per the assumptions of the MC approach (Toyoda et al., 2000). Consequently, a weighted mean D_e value has been calculated for these samples using the results obtained from the Al and Ti signals. This yields a combined D_e value of 970 ± 67 Gy for sample

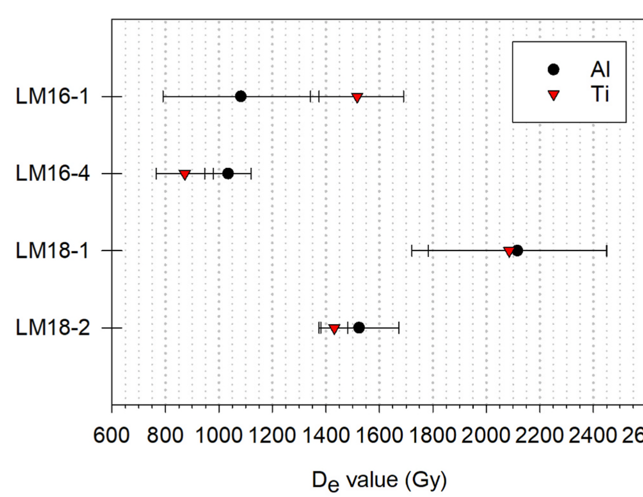

Fig. 3. Comparison of the quartz ESR D_e estimates obtained using the Al and Ti signals for the Tormes River terrace samples. The associated De uncertainties represent the 1σ ranges.

LM16-4, 1945 ± 199 Gy for sample LM18-1 and 1441 ± 48 Gy for sample LM18-2.

In contrast, sample LM16-1 shows an outlying pattern with D_e (Ti) > D_e (Al). Although the D_e values obtained for the two signals overlap within their uncertainty ranges, this apparent agreement should be treated with some caution as it mainly reflects the large associated D_e uncertainty ranges (11–27%), particularly for the Al signal, which act to mask a significant systematic inversion of 40% in the expected D_e relationships of the Ti and Al centres. The basic principles of the MC approach cannot explain this inverted D_e relationship because, all things being equal, it is not possible for the more rapidly bleached Ti signal to be reset to a lesser extent than the slower bleached Al signal prior to burial. We presently do not have an objective explanation for this unexpected result, though we cannot exclude the possibility that it might partly or wholly reflect the low quality of the ESR data for this sample; particularly the low repeatability of the measured D_e estimates, which varied by 39–54 % for the two signals (Table S12). In this context, the most conservative interpretation of the ESR dataset would be to consider the Al signal as providing a maximum constraint of 1082 ± 292 Gy for the true burial dose of LM16-1.

4.3. Final ages

The final luminescence ages obtained in this study are summarised in Table 1. For samples where both single-grain TT-OSL and multi-grain pIR-$IRSL_{225}$ ages have been obtained, all of the paired luminescence dating ages are in agreement at 1σ. Tera River sample BGN16-1 from the +30–35 m produces a combined TT-OSL and pIR-$IRSL_{225}$ age of 342 ± 27 ka, whilst the +16–20 m terrace samples (BGN16-2 and BGN16-3) yield combined ages of 237 ± 23 ka and 242 ± 21 ka, respectively. For the Tormes River terrace sequence, a multi-grain pIR-$IRSL_{225}$ age of 323 ± 19 ka is obtained for the +50 m terrace sample (LM18-2), while the combined TT-OSL and pIR-$IRSL_{225}$ ages for the +34 m and +14 m terraces show only modest age differentiation, ranging between 252 ± 23 ka and 244 ± 19 ka, and the +8 m terrace produces a systematically younger age of 219 ± 19 ka, as expected (Table 1). Finally, the multi-grain pIR-$IRSL_{225}$ ages obtained for the Guadiana River +8 m terrace samples (ALB17-1 and ALB17-2) are 252 ± 13 ka and 226 ± 15 ka, respectively, which result in a combined age of 242 ± 14 ka for the formation of this terrace.

The final ESR ages obtained for the Tormes River terraces are shown in Table 2. The combined Al–Ti ages are 402 ± 36 ka for sample LM16-4, 416 ± 49 ka for sample LM18-1 and 433 ± 28 ka for sample LM18-2. For sample LM16-1, only the Al signal is considered reliable (see previous section), producing an age of 288 ± 79 ka for the formation of the +50 m terrace.

5. Discussion and conclusion

5.1. Comparison of luminescence and ESR ages for the Tormes River deposits

The quartz samples from the Tormes River terraces produce weak TT-OSL signals, variable Al signal repeatability and below-average Ti signal fitting uncertainties. More encouragingly, the single-grain TT-OSL D_e distributions exhibit limited scattered and low-to-moderate overdispersion values, and are generally consistent with those reported elsewhere for well-bleached samples (e.g., Arnold et al., 2013, 2019, 2022; Demuro et al., 2023). The combined Al–Ti ESR age of 402 ± 36 ka obtained for sample LM16-4 (+8 m terrace) is significantly older than the corresponding single-grain TT-OSL age of 209 ± 25 ka, as well as the ~250 ka combined luminescence ages obtained for the +14 m terrace samples of (sample LM16-2 and LM16-3; Tables 1 and 2). This age overestimation may indicate that both the Al and Ti signals of sample LM16-4 were not fully reset prior to deposition, and we therefore favour the luminescence ages produced for this sample.

For sample LM16-1, and following the principles of the MC approach, the ESR age estimate of 288 ± 79 ka should be regarded as a maximum possible age because it is based on the Al signal alone. This age is compatible with the corresponding single-grain quartz TT-OSL age of 249 ± 24 ka obtained for this sample, as well as the combined extended-range luminescence age of 252 ± 23 ka (Table 1). Interestingly, the Ti–H signal, which is typically better suited for late Middle Pleistocene samples (e.g., Bartz et al., 2020), provides a D_e estimate of 734 ± 134 Gy for this sample, resulting in an age of 195 ± 37 ka (Table S13). This age should be treated with some caution given the low goodness-of-fit value obtained for the Ti–H dose response curve fitting, though it is consistent at 2σ with the single-grain TT-OSL age obtained for LM16-1 (albeit systematically younger by ~55 ka). Furthermore, since the magnitude of the Ti–H D_e estimate lies beyond the range (0–300 Gy) usually considered suitable for this signal (Duval et al., 2020b), the resulting Ti–H ESR age should be regarded as a minimum estimate of the true depositional age. Consequently, the ESR Ti–H and Al ages provide bracketing minimum and maximum constraints for the +34 m terrace, and support the finite single-grain TT-OSL and multi-grain pIR-IRSL ages obtained for these deposits.

The combined ESR age of 424 ± 12 ka for the +50 m terrace samples (LM18-1 and LM18-2) is older than the corresponding pIR-$IRSL_{225}$ age of 323 ± 19 ka, which may be compatible with the observation that the natural pIR-$IRSL_{225}$ signal is close to saturation (**e.g.,** Fig. 2c), and thus may be yielding a minimum age estimate for the terrace formation. However, we cannot completely exclude the possibility that the true age of the +50 m deposits is younger than the mean ESR age due to the possibility of insufficient Al and Ti signal resetting (i.e., the Tormes +50 m terrace age may be between ~330 ka and ~420 ka). This may be a valid concern given that the ESR results for sample LM16-4, collected from the +8 m terrace, suggest that the Al and Ti signals of related Tormes River fluvial deposits may not have been fully reset during sediment transport.

5.2. New and revised chronological frameworks for Iberian fluvial terraces

The two pIR-$IRSL_{225}$ ages obtained for the Guadiana River terrace at +8 m suggest it formed 242 ± 14 ka (combined ages for samples ALB17-1 and ALB17-2; Table 1), towards the end of marine isotope stage (MIS) 8 or the beginning of MIS 7 (Lisiecki and Raymo, 2005). This age range overlaps with those obtained for the lower terraces (+8 m to +20 m) of the Tormes and Tera River in the Duero basin (i.e., ~220 to ~250 ka), which would imply stagnated incision for the Guadiana River when compared to rivers in the Duero basin. However, our ages for the fluvial terraces in the middle section of the Duero basin also indicate certain differences exist in the timing of fluvial terrace formation among the various tributaries located to the north and south of the Duero River. For the Tera River on the northern flank of the basin, the +16–20 m to +30–35 m terraces formed approximately 240 ± 22 ka and 342 ± 27 ka, respectively, most likely during MIS 10 and MIS 8 to 7. The Tera River +30–35 m terrace is comparatively older than its equivalent for the Tormes River on the southern flank of the basin, where the +34 m terrace is luminescence dated to 252 ± 23 ka, during MIS 8 or 7. Additionally, the Tormes River +50 m terrace age of 323–433 ka (combined ESR and luminescence age range), coinciding with MIS 11 to 9, implies a different (faster) terrace incision rate for this section of the Tormes River when compared to the Tera River.

Previous studies have also produced slightly older ages for equivalent +30 m terraces along other tributaries of the Duero River. Moreno et al. (2012), for instance, reported quartz Al ESR ages of 370 ± 10 ka and 400 ± 90 ka for the +26–35 m terrace of the Arlanzón River, and an Al ESR age of 350 ± 4 ka for the +33–36 m terrace of the Arlanza River (Moreno et al., 2016), both of which are located in the headwaters of the Duero basin. Given the potential for incomplete bleaching of the Al ESR signal, which is evident from sample LM16-4 and other comparative dating studies of Iberian fluvial deposits (e.g., Level PM3 in Méndez-Quintas et al., 2018; Duval et al., 2017), it may be prudent to interpret the Al ESR ages of Moreno et al. (2012) and Moreno et al. (2016) as maximum age estimates. The recent luminescence dating study of the +20–23 m terrace in the Pisuerga River valley (a tributary of the Duero located in the northeast of the basin) also presented a combined TT-OSL and pIR-IRSL$_{225}$ age of ~300 ka (Terradillos-Bernal et al., 2023), which is older than the age obtained in the present study for terraces of equivalent elevation. Importantly, the replicate ages of 252 ± 23 ka (combined luminescence age) and the maximum age of 288 ± 79 ka (ESR Al signal) obtained for the Tormes River +34 m terrace in the current study indicate general agreement when using different dating methods, signals, minerals, and scales of D_e analysis; thus providing good support for the reliability of the dating procedures employed here, and underscoring the potentially complex age-elevation relationships in different tributaries of the Duero basin.

Comparison of these published chronological datasets, as well as our latest dating results, point to some fluvial terraces of the Duero basin potentially having diachronous formation histories. The propensity for complex response behaviours, inherent morphological adjustments

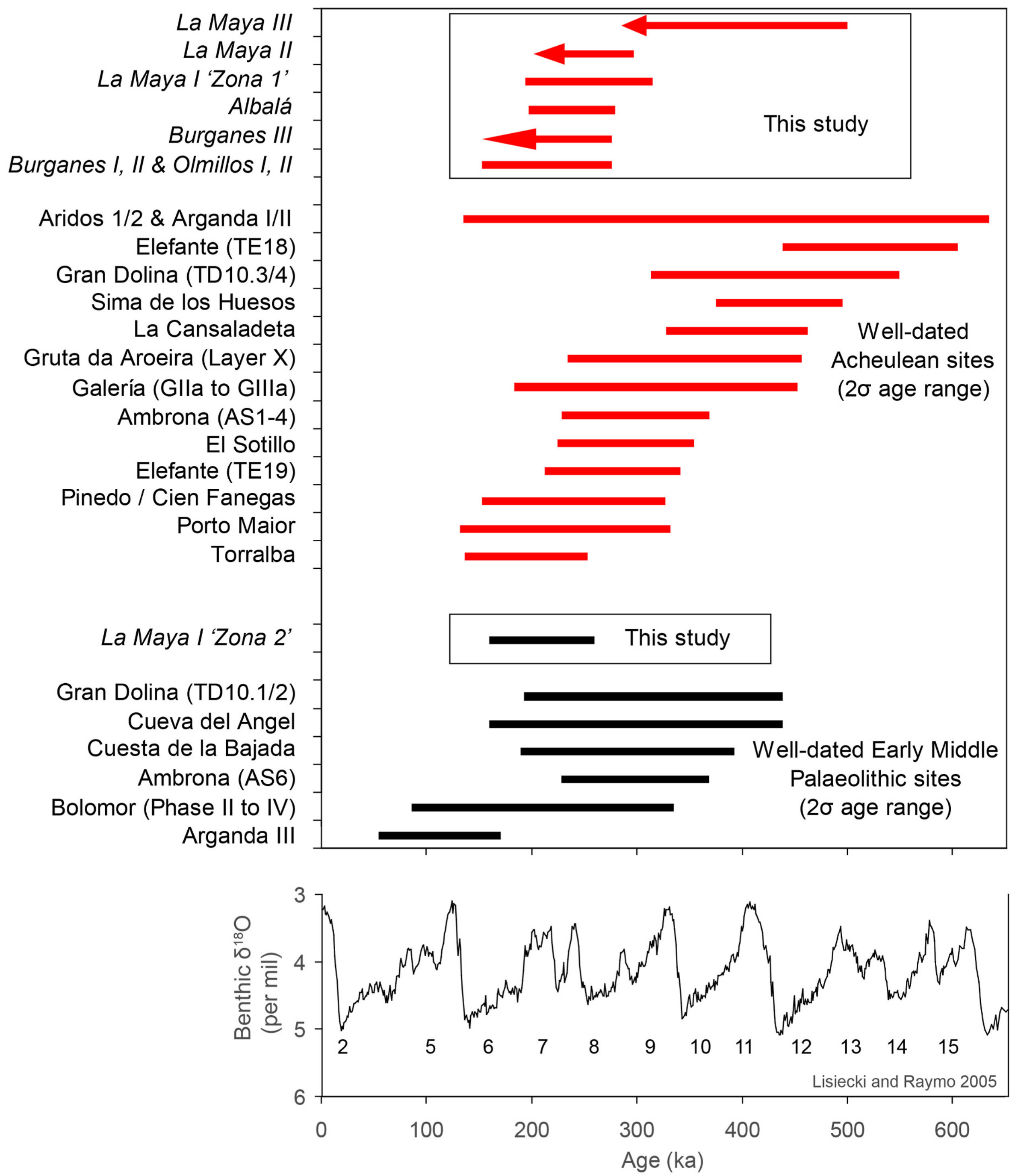

Fig. 4. Age ranges of well-known archaeological sites from the Iberian Peninsula with industries classed as Acheulean and early Middle Palaeolithic. The individual chronologies for each site and the plotted age ranges displayed here are summarised in Table S14 and are based on the work presented here and previously published studies. The site Barranc de la Boella is not plotted because its age falls beyond the maximum x-axis value (i.e., >650 ka). Also shown for reference is the marine oxygen isotope curve of Lisiecki and Raymo (2005). Arrows indicate that the numerical ages obtained from the terrace deposits represent maximum ages for the surficial archaeological assemblages at these sites.

following the exceedance of intrinsic critical slope stability thresholds, and time-transgressive adjustments to base level changes over different parts of large basins such as the Duero (e.g., Schumm and Parker, 1973; Bull, 1991), dictate that it is unlikely fluvial terrace formation occurred coevally across the entire region and that minor age variations between different sections of the basin may be expected. Irrespective, our results add to the body of evidence suggesting that the middle elevation fluvial terraces (+30 m through to +8 m) of the Duero basin likely formed during the last third of the Middle Pleistocene, post-MIS 10.

Finally, the depositional age of the Tormes River +50 m terrace is constrained to between 323 ± 19 ka (from pIR-IRSL$_{225}$ of LM18-2) and 424 ± 12 ka (combined Al and Ti ESR ages of samples LM18-1 and LM18-2), which is younger than the previously published quartz Al ESR ages of 600–700 ka obtained for an equivalent terrace elevation in the Arlanzón River basin (Moreno et al., 2012). However, given the potential complications that can arise from insufficient resetting of the Al ESR signal, which are difficult to assess in the absence of comparative Ti centre data, it is necessary to interpret the latter ages with some caution (i.e., they should probably be regarded as maximum ages). Despite this caveat, the results presented here and in previous studies suggest that the +50 m terraces of the Duero basin likely formed during MIS 10 or earlier.

5.3. Implications for lower Palaeolithic records of Iberia

The Middle Pleistocene Lower Palaeolithic records of the Iberian Peninsula are characterised by an Acheulean industry composed of large cutting tools (LCT; Santonja and Villa, 2006; Méndez-Quintas et al., 2018); i.e., handaxes and cleavers of large format (frequently upward of ~15 cm in length). In Western Europe, the geographical distribution of these records is limited to Iberia and southwest France, in the Aquitaine region (Santonja and Villa, 2006; Santonja et al., 2016). Chronologies for the Acheulean in Iberia typically span the second half of the Middle Pleistocene, between ~500 and ~200 ka. Fig. 4 shows a summary of published ages for Acheulean sites in Iberia and their relationship with the results obtained in the present study (age ranges are presented with their 2σ uncertainties; see Table S14 for site summaries). For La Maya II, La Maya III and Burganes III, in which archaeological material was recovered from surficial deposits of the Tormes and Tera River terraces, we can only determine that these archaeological records are younger than ~296 ka, ~516 ka and ~276 ka, respectively (i.e., the maximum age of underlying terraces, with their age ranges considered at 2σ). The age range (luminescence dating only) of sites where Acheulean archaeological material has been found or excavated *in situ*, which includes La Maya I 'Zona 1' (193–314 ka), Burganes I–II and Olmillos I–II (151–276 ka), and Albalá (196–278 ka), indicate these sites fall within the MIS 9–7 timeframe, squarely overlapping with ages obtained for well-known Acheulean sites in the region, including Porto Maior, El Sotillo and Ambrona (AS 1–4) (Fig. 4; Table S14). In contrast, the industry represented at La Maya I 'Zona 2' site shows deviations from the Acheulean and possibly belongs to what has been described as the early Middle Palaeolithic (EMP) (see Santonja and Perez-Gonzalez, 1984; Santonja et al., 2016); an industry characterised by retouched tools on flake and very few LCTs (Santonja et al., 2016; Santonja et al., 2014). The 159–259 ka age range determined for this industry at La Maya I 'Zona 2' (Table S14), which is centred on MIS 7, agrees with chronologies obtained for other EMP sites of Iberia, such as Gran Dolina (TD10.1/2), Cuesta de la Bajada, Cueva del Angel and Bolomor (phase II) (Fig. 4).

The new and previously published chronological datasets for Iberian Acheulean and EMP sites indicate these two industries are dated to the last part of the Middle Pleistocene. Thus, our study confirms previous observations regarding the chronological overlap of these two technologies in the region and their likely coexistence during the last third of the Middle Pleistocene, indicating a possible non-linear pattern of replacement for the Acheulean (LCT) in the Iberian Peninsula during the Lower to Middle Palaeolithic transition (Santonja et al., 2016).

CRediT authorship contribution statement

Martina Demuro: Conceptualization, Data curation, Formal analysis, Funding acquisition, Investigation, Methodology, Writing – original draft, Writing – review & editing. **Lee J. Arnold:** Conceptualization, Data curation, Formal analysis, Funding acquisition, Investigation, Methodology, Writing – original draft, Writing – review & editing. **Mathieu Duval:** Conceptualization, Formal analysis, Investigation, Methodology, Writing – original draft, Writing – review & editing. **Alicia Churruca Clemente:** Data curation, Formal analysis, Methodology. **Manuel Santonja:** Conceptualization, Investigation, Writing – original draft, Writing – review & editing, Resources. **Alfredo Pérez-González:** Investigation, Methodology, Writing – original draft, Writing – review & editing.

Declaration of competing interest

The authors declare that they have no known competing financial interests or personal relationships that could have appeared to influence the work reported in this paper.

Data availability

Data will be made available on request.

Acknowledgements

The luminescence dating research undertaken by Martina Demuro was supported by Australian Research Council (ARC) Future Fellowship FT200100816 and ARC Discovery Early Career Researcher Award DE160100743. Mathieu Duval is currently supported by the Spanish Ramón y Cajal Fellowship RYC2018-025221-I funded by MCIN/AEI/10.13039/501100011033 and by 'ESF Investing in your future'. This work is associated with Grant PID2021-123092NB-C22 funded by MCIN/AEI/10.13039/501100011033/'ERDF A way of making Europe'. The authors would like to thank G. Ross and R. Power, University of Adelaide, and C. García Rodríguez and M.J. Alonso Escarza, CENIEH, for their technical support with the luminescence and ESR dating analytical procedures.

Appendix A. Supplementary data

Supplementary data to this article can be found online at https://doi.org/10.1016/j.quageo.2024.101567.

References

Aitken, M., 1998. An Introduction to Optical Dating: the Dating of Quaternary Sediments by the Use of Photon-Stimulated Luminescence. Oxford University Press, Oxford, p. 267.

Arnold, L.J., Roberts, R.G., 2009. Stochastic modelling of multi-grain equivalent dose (D_e) distributions: implications for OSL dating of sediment mixtures. Quat. Geochronol. 4, 204–230.

Arnold, L.J., Roberts, R.G., Galbraith, R.F., DeLong, S.B., 2009. A revised burial dose estimation procedure for optical dating of young and modern-age sediments. Quat. Geochronol. 4, 306–325.

Arnold, L.J., Duval, M., Falguères, C., Bahain, J.-J., Demuro, M., 2012a. Portable gamma spectrometry with cerium-doped lanthanum bromide scintillators: suitability assessments for luminescence and electron spin dating applications. Radiat. Meas. 47, 6–18.

Arnold, L.J., Demuro, M., Navazo Ruiz, M., 2012b. Empirical insights into multi-grain averaging effects from 'pseudo' single-grain OSL measurements. Radiat. Meas. 47, 652–658.

Arnold, L.J., Demuro, M., Navazo, M., Benito-Calvo, A., Pérez-González, A., 2013. OSL dating of the Middle Palaeolithic Hotel California site, Sierra de Atapuerca, north-central Spain. Boreas 42, 285–305.

Arnold, L.J., Demuro, M., Spooner, N.A., Prideaux, G.J., McDowell, M.C., Camens, A.B., Reed, E.H., Parés, J.M., Arsuaga, J.L., Bermúdez de Castro, J.M., Carbonell, E., 2019.

Single-grain TT-OSL bleaching characteristics: insights from modern analogues and OSL dating comparisons. Quat. Geochronol. 49, 45–51.
Arnold, L.J., Demuro, M., Parés, J.M., Arsuaga, J.L., Aranburu, A., Bermúdez de Castro, J.M., Carbonell, E., 2014. Luminescence dating and palaeomagnetic age constraint on hominins from Sima de los Huesos, Atapuerca, Spain. J. Human Evol. 67, 85–107.
Arnold, L.J., Demuro, M., Parés, J.M., Pérez-González, A., Arsuaga, J.L., Bermúdez de Castro, J.M., Carbonell, E., 2015. Evaluating the suitability of extended-range luminescence dating techniques over Early and Middle Pleistocene timescales: Published datasets and case studies from Atapuerca, Spain. Quat. Int. 389, 167–190.
Arnold, L.J., Demuro, M., Power, R., Priya1, Duval, M., Guilarte, V., Weij, R., Woodhead, J., White, L., Bourne, S., Reed, E.H., 2022. Examining sediment infill dynamics at Naracoorte Cave megafauna sites using multiple luminescence dating signals. Quat. Geochronol. 70, 101301.
Arroyo, A., de la Torre, I., 2013. Acheulean large flake technology in Campo de Calatrava (Ciudad Real, Spain). Archaeol. Ethnol. Anthropol. Eurasia 41, 2–10.
Bailey, R.M., Arnold, L.J., 2006. Statistical modelling of single grain quartz De distributions and an assessment of procedures for estimating burial dose. Quat. Sci. Rev. 25, 2475–2502.
Bartz, M., Duval, M., Brill, D., Zander, A., King, G.E., Rhein, A., Walk, J., Stauch, G., Lehmkuhl, F., Brückner, H., 2020. Testing the potential of K-feldspar postIR-IRSL and quartz ESR for dating coastal alluvial fan complexes in arid environments. Quat. Int. 556, 124–143.
Bull, W.B., 1991. Geomorphic Responses to Climatic Change. Oxford University Press, Oxford, p. 326.
Buylaert, J.-P., Jain, M., Murray, A.S., Thomsen, K.J., Thiel, C., Sohbati, R., 2012. A robust feldspar luminescence dating method for Middle and Late Pleistocene sediments. Boreas 41, 435–451.
Cunha, P.P., Martins, A.A., Huot, S., Murray, S., Raposo, L., 2008. Dating the Tejo river lower terraces in the Ródão area (Portugal) to assess the role of tectonics and uplift. Geomorphology 102, 43–54.
Demuro, M., Arnold, L.J., Parés, J.M., Pérez-González, A., Ortega, A.I., Arsuaga, J.L., Bermúdez de Castro, J.M., Carbonell, E., 2014. New luminescence ages for the Galería Complex archaeological site: Resolving chronological uncertainties on the Acheulean record of the Sierra de Atapuerca, northern Spain. PLoS One 9 (10), e110169.
Demuro, M., Arnold, L.J., Parés, J.M., Sala, R., 2015. Extended-range luminescence chronologies suggest potentially complex bone accumulation histories at the Early-to-Middle Pleistocene palaeontological site of Huéscar-1 (Guadix-Baza basin, Spain). Quat. Int. 389, 191–212.
Demuro, M., Arnold, L.J., Aranburu, A., Sala, N., Arsuaga, J.L., 2019. New bracketing luminescence ages constrain the Sima de los Huesos hominin fossils (Atapuerca, Spain) to MIS 12. J. Hum. Evol. 131, 76–95.
Demuro, M., Arnold, L.J., Aranburu, A., Gómez-Olivencia, A., Arsuaga, J.L., 2019a. Single-grain OSL dating of the Middle Palaeolithic site of Galería de las Estatuas, Atapuerca (Burgos, Spain). Quat. Geochronol. 49, 254–261.
Demuro, M., Arnold, L.J., Duval, M., Méndez-Quintas, E., Santonja, M., Pérez-González, A., 2020a. Refining the chronology of Acheulean deposits at Porto Maior in the River Miño basin (Galicia, Spain) using a comparative luminescence and ESR dating approach. Quat. Int. 556, 96–112.
Demuro, M., Duval, M., Arnold, L.J., Spooner, N.A., Ceighton, D.F., Méndez-Quintas, E., Santonja, M., Pérez-González, A., 2020b. Insights into the relationship between luminescence and ESR dating signals from Spanish sedimentary quartz samples of different geologic origins. Quat. Int. 556, 165–179.
Demuro, M., Arnold, L.J., Parés, J.M., Aranburu, A., Huguet, R., Vallverdú, J., Arsuaga, J. L., Bermúdez de Castro, J.M., Carbonell, E., 2022. Extended-range luminescence chronologies for the Middle Pleistocene units at the Sima del Elefante archaeological site (Sierra de Atapuerca, Burgos, Spain). Quat. Geochronol. 71, 101318.
Demuro, M., Arnold, L.J., González-Urquijo, J., Lazuen, T., Frochoso, M., 2023. Chronological constraint of Neanderthal cultural and environmental changes in southwestern Europe. MIS 5–MIS 3 dating of the Axlor site (Biscay, Spain). J. Quat. Sci. 38, 891–920.
Duval, M., Guilarte, V., 2015. ESR dosimetry of optically bleached quartz grains extracted from Plio-Quaternary sediment: evaluating some key aspects of the ESR signals associated to the Ti-centers. Radiat. Meas. 78, 28–41.
Duval, M., Arnold, L.J., Guilarte, V., Demuro, M., Santonja, M., Pérez-González, A., 2017. Electron Spin Resonance dating of optically bleached quartz grains from the Middle Palaeolithic site of Cuesta de la Bajada (Spain) using the multiple centres approach. Quat. Geochronol. 37, 82–96.
Duval, M., Voinchet, P., Arnold, L.J., Parés, J.M., Minnella, W., Guilarte, V., Demuro, M., Falguères, C., Bahain, J.-J., Despriée, J., 2020a. A multi-technique dating study sheds new light on the chronology of two Lower Palaeolithic sites of the Middle Loire Basin, France: lunery-la Terre-des-Sablons and Brinay-la Noira. Quat. Int. 556, 79–95.
Duval, M., Arnold, L.J., Rixhon, G., 2020b. Electron Spin Resonance Dating in Quaternary studies: evolution, recent advances and applications. Quat. Int. 556, 1–10.
Duval, M., Arnold, L.J., 2013. Field gamma dose-rate assessment in natural sedimentary contexts using LaBr3(Ce) and NaI(Tl) probes: A comparison between the "threshold" and "windows" techniques. Appl. Radiat. Isot. 74, 36–45.
Duval, M., Guilarte Moreno, V., Bartz, M., Alonso Escarza, M.J., Ben Arous, E., del Val, M., García Rodríguez, C., 2024. ESR dating of quartz grains: evaluating measurement repeatability and reproducibility. Radiat. Phys. Chem. 111313 https://doi.org/10.1016/j.radphyschem.2023.111313.
Galbraith, R.F., Roberts, R.G., Laslett, G.M., Yoshida, H., Olley, J.M., 1999. Optical dating of single and multiple grains of quartz from Jinmium rock shelter, northern Australia: Part I, experimental design and statistical models. Archaeometry 41, 339–364.
García-Vadillo, F.-J., Carbonell, E., Rodríguez-Álvarez, X.-P., Barsky, D., Canals-Salomó, A., 2023. The technological multiplicity of the acheulean of the southern iberian Peninsula. L'anthropologie 127, 103113.
Guérin, G., Mercier, M., Adamiec, G., 2011. Dose-rate conversion factors: update. Ancient TL 29, 5–8.
Guilarte, V., Duval, M., 2021. ESR dating of optically bleached quartz grains: intra-laboratory comparison of different experimental setups and their impact on dose evaluation. Geochronometria 48, 179–190.
Huntley, D.J., Baril, M.R., 1997. The K content of the K-feldspars being measured in optical dating or in thermoluminescence dating. Ancient TL 15, 11–13.
Huntley, D.J., Hancock, R.G.V., 2001. The Rb contents of the K-feldspar grains being measured in optical dating. Ancient TL 19, 43–46.
Joannes-Boyau, R., Duval, M., Bodin, T., 2018. MCDoseE 2.0: a new Markov chain Monte Carlo program for ESR dose response curve fitting and dose evaluation. Quat. Geochronol. 44, 13–22.
Laplana, C., Herráez, E., Yravedra Saínz de los Terreros, J., Bárez, S., Rubio-Jara, S., Panera, J., Rus, I., Pérez-González, A., 2015. Biochronology of the complex terrace of butarque of the manzanares River at the stormwater tank in southern Madrid (Spain). Estud. Geol. 71 (1), e028.
Lisiecki, L.E., Raymo, M.E., 2005. A Pliocene-Pleistocene stack of 57 globally distributed benthic δ18O records. Paleoceanography 20. PA 1003.
López-Recio, M., Silva, P.G., Roquero, E., Cunha, P.P., Tapias, F., Alcaraz-Castaño, M., Baena, J., Cuartero, F., Morín, J., Torres, T., Ortiz, J.E., Murray, A.S., Buylaert, J.P., 2015. Geochronology of the acheulean sites of pinedo and cien fanegas (Tagus River valley), and implications for the fluvial evolution in the environs of toledo (Spain). Estud. Geol. 71 (1), e029.
Martins, A.A., Cunha, P.P., Hout, S., Murray, A.S., Buylaert, J.P., 2009. Geomorphological correlation of the tectonically displaced Tejo River terraces (Gavião–Chamusca area, central Portugal) supported by luminescence dating. Quat. Int. 199, 75–91.
Martins, A.A., Cunha, P.P., Buylaert, J.P., Hout, S., Murray, A.S., Dinis, P., Stokes, M., 2010. K-feldspar IRSL dating of a Pleistocene river terrace staircase sequence of the Lower Tejo River (Portugal, western Iberia). Quat. Geochronol. 5, 176–180.
Méndez-Quintas, E., Santonja, M., Pérez-González, A., Duval, M., Demuro, M., Arnold, L. J., 2018. First evidence of an extensive Acheulean large cutting tool accumulation in Europe from Porto Maior (Galicia, Spain). Sci. Rep. 8, 3082.
Méndez-Quintas, E., Demuro, M., Arnold, L.J., Duval, M., Santonja, M., Pérez-González, A., 2019. Insights into the late stages of the acheulean technocomplex of western Iberia from the arbo site (galicia, Spain). J. Archaeol. Sci.: Reports 27, 101934.
Moreno, D., Falguères, C., Pérez-González, A., Duval, M., Voinchet, P., Benito-Calvo, A., Ortega, A.I., Bahain, J.-J., Sala, R., Carbonell, E., Bermúdez de Castro, J.M., Arsuaga, J.L., 2012. ESR chronology of alluvial deposits in the Arlanzon valley (Atapuerca, Spain): contemporaneity with Atapuerca Gran Dolina site. Quat. Geochronol. 10, 418–423.
Moreno, D., Benito-Calvo, A., Falguères, C., Voinchet, P., Pérez-González, A., 2016. Datación preliminar por ESR de la secuencia de terrazas fluviales del valle del Arlanza (Sector NE de la Cuenca del Duero, Burgos). In: XIV Reunión Nacional de Geomorfología, pp. 391–398. Málaga.
Moreno, D., Duval, M., Rubio-Jara, S., Panera, J., Bahain, J.-J., Shao, Q., Pérez-González, A., Falguères, C., 2019. ESR dating of Middle Pleistocene archaeo-paleontological sites from the Manzanares and Jarama river valleys (Madrid basin, Spain). Quat. Int. 520, 23–38.
Murray, A.S., Wintle, A., 2000. Luminescence dating of quartz using an improved single-aliquot regenerative-dose protocol. Radiat. Meas. 32, 57–73.
Panera, J., Torres, T., Pérez-González, A., Ortiz, J.E., Rubio-Jara, S., Uribelarrea del Val, D., 2011. Geochronology of the arganda complex terrace in the jarama River valley (madrid, Spain). Estud. Geol. 67, 495–504.
Panera, J., Rubio-Jara, S., Yravedra, J., Blain, H.-A., Sesé, C., Pérez-González, A., 2014. Manzanares Valley (madrid, Spain): a good country for proboscideans and neanderthals. Quat. Int. 326–327, 329–343.
Portero, J.M., Ramírez Merino, J.L., Aconchea Soto, E., Barón, J.M., Monteserín López, V., 1986. MAGNA. E. 1:50.000. Hoja 759. Piedrabuena.
Prescott, J.R., Hutton, J.T., 1994. Cosmic ray contributions to dose rates for luminescence and ESR dating: large depths and long-term time variations. Radiat. Meas. 23, 497–500.
Rios-Garaizar, J., Iriarte, E., Arnold, L.J., Sánchez-Romero, L., Marín-Arroyo, A.B., San Emeterio, A., Gómez-Olivencia, A., Pérez-Garrido, C., Demuro, M., Campaña, I., Bourguignon, L., Benito-Calvo, A., Iriarte, M.J., Aranburu, A., Arranz-Otaegi, A., Garate, D., Silva-Gago, M., Lahaye, C., Ortega, I., 2022. The intrusive nature of the chatelperronian in the iberian Peninsula. PLoS One 17 (3), e0265219.
Rubio-Jara, S., Panera, J., Rodríguez-de-Tembleque, J., Santonja, M., Pérez-González, A., 2016. Large flake Acheulean in the middle of Tagus basin (Spain): middle stretch of the river Tagus valley and lower stretches of the rivers Jarama and Manzanares valleys. Quat. Int. 411, 349–366.
Santamaría, M., Navazo, M., Arnold, L.J., Benito-Calvo, A., Demuro, M., Carbonell, E., 2023. Low-cost technologies in a rich ecological context: Hotel California open-air site at Sierra de Atapuerca, Burgos, Spain. J. Quat. Sci. 38, 658–684.
Santonja, M., Pérez-González, A., 1984. Las industrias paleolíticas de La Maya I en su ámbito regional. In: Excavaciones Arqueológicas en España, vol 135. Ministerio de Cultura, Madrid.
Santonja, M., Pérez-González, A., 2010. Mid-pleistocene acheulean industrial complex in the iberian Peninsula. Quat. Int. 223–224, 154–161.

Santonja, M., Pérez-González, A., Panera, J., Rubio-Jara, S., Méndez-Quintas, E., 2016. The coexistence of Acheulean and Ancient Middle Palaeolithic techno-complexes in the Middle Pleistocene of the Iberian Peninsula. Quat. Int. 411, 367–377.

Santonja, M., Villa, P., 2006. The acheulean in southwestern Europe. In: Goren-Inbar, N., Sharon, G. (Eds.), Axe Age. Acheulian Tool-Making from Quarry to Discard. Equinox Publishing, London, p. 429e478.

Santonja, M., Pérez-González, A., Baena, J., Panera, J., Méndez-Quintas, E., Uribelarrea, D., Demuro, M., Arnold, L., Abrunhosa, A., Rubio-Jara, S., 2022. The Acheulean of the upper Guadiana River Basin (Central Spain). morphostratigraphic context and chronology. Front. Earth Sci. 10, 912007.

Santonja, M., Pérez-González, A., Domínguez-Rodrigo, M., Panera, J., Rubio-Jara, S., Sesé, C., Soto, E., Arnold, L.J., Duval, M., Demuro, M., Ortiz, J.E., Torres, T. de, Mercier, N., Barba, R., Yravedra, J., 2014. The Middle Paleolithic site of Cuesta de la Bajada (Teruel, Spain): A perspective on the Acheulean and Middle Paleolithic technocomplexes in Europe. J. Archaeol. Sci. 49, 556-571.

Schumm, S.A., Parker, R.S., 1973. Implications of complex response of drainage systems for Quaternary alluvial stratigraphy. Nature 243, 99–100.

Terradillos-Bernal, M., Demuro, M., Arnold, L.J., Jordá-Pardo, J.F., Clemente-Conte, I., Benito-Calvo, A., Díez Fernández-Lomana, J.C., 2023. San quirce (palencia, Spain): new chronologies for the lower to middle palaeolithic transition of south-west Europe. J. Quat. Sci. 38, 21–37.

Toyoda, S., Falguères, C., 2003. The method to represent the ESR signal intensity of the aluminium hole center in quartz for the purpose of dating. Adv. ESR Appl. 20, 7–10.

Toyoda, S., Voinchet, P., Falguères, C., Dolo, J.M., Laurent, M., 2000. Bleaching of ESR signals by the sunlight: a laboratory experiment for establishing the ESR dating of sediments. Appl. Radiat. Isot. 52, 1357–1362.